Volume 8 · No. 12 – June 25 2012

NANO **small** MICRO

www.small-journal.com

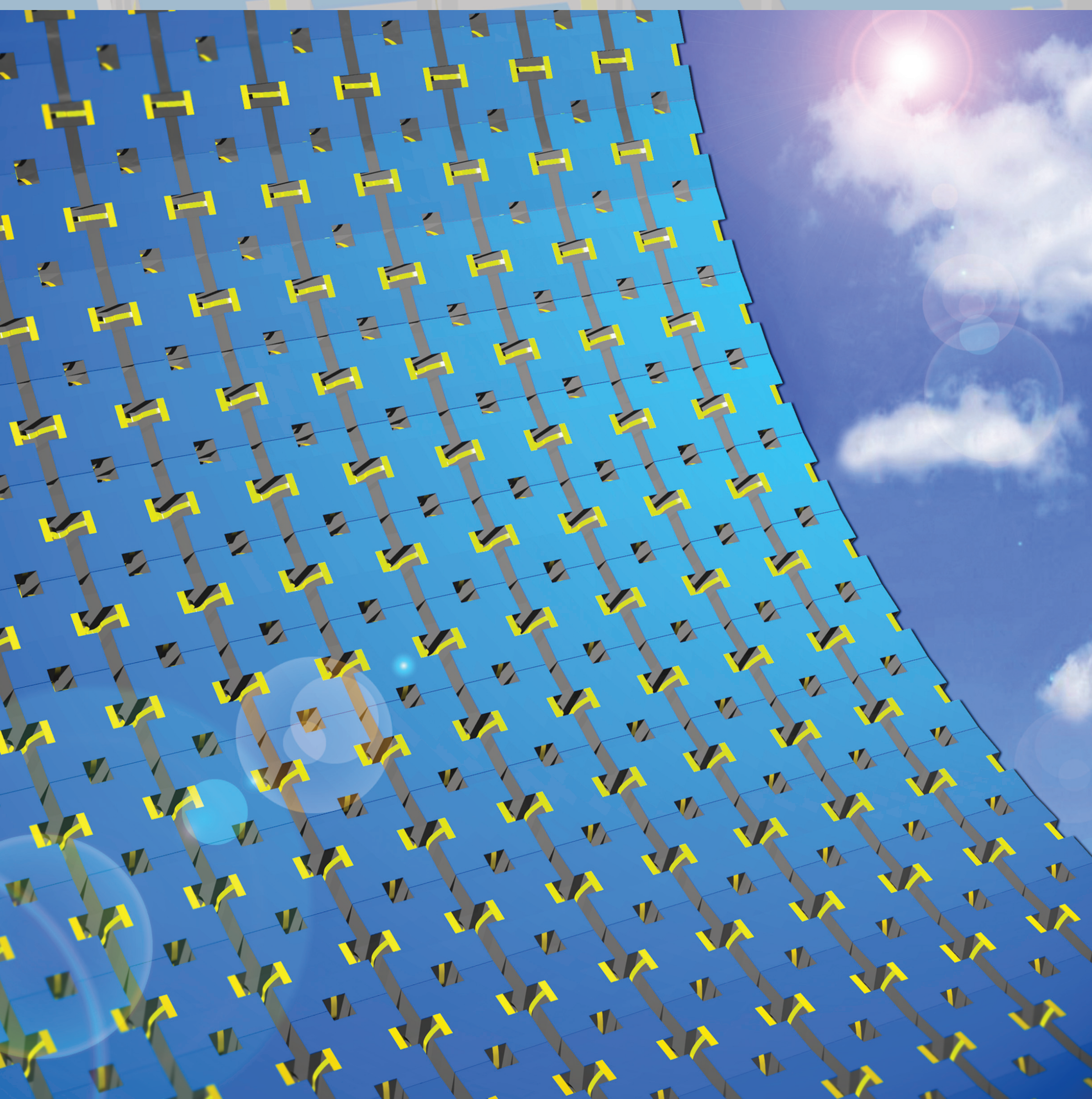

12/2012

WILEY-VCH

Stretchable Semiconductor Technologies with High Areal Coverages and Strain-Limiting Behavior: Demonstration in High-Efficiency Dual-Junction GaInP/GaAs Photovoltaics

J. A. Rogers et al.

Stretchable Semiconductor Technologies with High Areal Coverages and Strain-Limiting Behavior: Demonstration in High-Efficiency Dual-Junction GaInP/GaAs Photovoltaics

*Jongho Lee, Jian Wu, Jae Ha Ryu, Zhuangjian Liu, Matthew Meitl, Yong-Wei Zhang, Yonggang Huang, and John A. Rogers**

Recent research has uncovered ways to build mechanically flexible or even stretchable electronic/optoelectronic systems with inorganic materials, including those, such as monocrystalline silicon and gallium arsenide, whose electrical performance and reliability characteristics in devices and circuits are well established, due to decades of work in the semiconductor industry.[1–9] The resulting classes of flexible/stretchable technologies exploit heterogeneous integration of high- and low-modulus inorganic and organic materials, respectively, to overcome design constraints set by the platforms used for traditional semiconductor components, i.e., planar, rigid and brittle semiconductor wafers.[10–17] Several concepts are now available for integrating micro- and nanoscale inorganic devices, often based on active materials in micro-/nanomembrane formats,[18] onto stretchable supports, to create opportunities in flexible display,[19–21] curvilinear digital cameras,[22–24] bio-integrated electronic monitors and therapeutic devices,[25–27] and many others. Mechanical designs that isolate strains associated with applied deformations away from brittle, inorganic constituent materials, to other components of the system are critically important. Most schemes involve some means to trade out-of-plane displacements of mechanically buckled structures, for in-plane relative motions of constituent devices.[28] One advanced approach that builds on this idea exploits geometrically structured substrates, in configurations where the devices mount on raised islands and the interconnects between them buckle downward into separating trenches.[29] Here, the trench regions absorb most of the externally applied strains, whereas the top surfaces of the islands barely deform, resulting in minimal interfacial stresses transmitted to devices mounted on top. A key advantage, compared to other schemes, is the ability to maintain high areal coverages in active devices, for areas of application, such as photodetection and photovoltaics, where such layouts are important. Here, we present an elaboration on this scheme that not only further increases the degree of stretchability and the areal coverage, but also provides a natural form of strain-limiting behavior, to help avoid destructive effects of extreme deformations. Experimental and theoretical studies describe the underlying mechanics. Epitaxially grown, dual-junction GaInP/GaAs solar cells with microscale dimensions and ultrathin forms enable demonstrations in integrated stretchable photovoltaic modules with high power conversion efficiencies. The high performance enabled by dual-junction GaInP/GaAs microcells improves the chances for realistic use of these modules, compared to the previously reported single-junction counterparts.[29] In addition, the results demonstrate the versatility of the reported mechanics designs, by illustrating their compatibility with thick, brittle semiconductor devices.

Advanced designs in structured elastomeric substrates, as shown in **Figure 1**, involve relief in the form of raised islands with rectangular notches in the central regions of the four edges, to provide a surface for mounting interconnected arrays of microscale solar cells (microcells) in a manner that yields

Prof. J. Lee
Department of Mechatronics
Gwangju Institute of Science and Technology (GIST)
123 Cheomdan-gwagiro
Buk-gu, Gwangju, 500-712, Korea
Prof. J. Wu
Department of Engineering Mechanics
Tsinghua University
Beijing, 100084, China
J. H. Ryu
Department of Materials Science and Engineering
Frederick Seitz Materials Research Laboratory
University of Illinois at Urbana-Champaign Urbana, IL 61801, USA
Z. Liu, Y.-W. Zhang
Institute of High Performance Computing
1 Fusionopolis Way, #16-16 Connexis, 138632, Singapore
Dr. M. Meitl
Semprius, 4915 Prospectus Dr., Durham, NC 27713, USA
Prof. Y. Huang
Department of Mechanical Engineering
Civil and Environmental Engineering
Northwestern University
Evanston, IL 60208, USA
Prof. J. A. Rogers
Department of Materials Science and Engineering
Department of Chemistry
Department of Mechanical Science and Engineering
Department of Electrical and Computer Engineering
Frederick Seitz Materials Research Laboratory
Beckman Institute for Advanced Science and Technology
University of Illinois at Urbana-Champaign Urbana, IL 61801, USA
E-mail: jrogers@uiuc.edu

DOI: 10.1002/smll.201102437

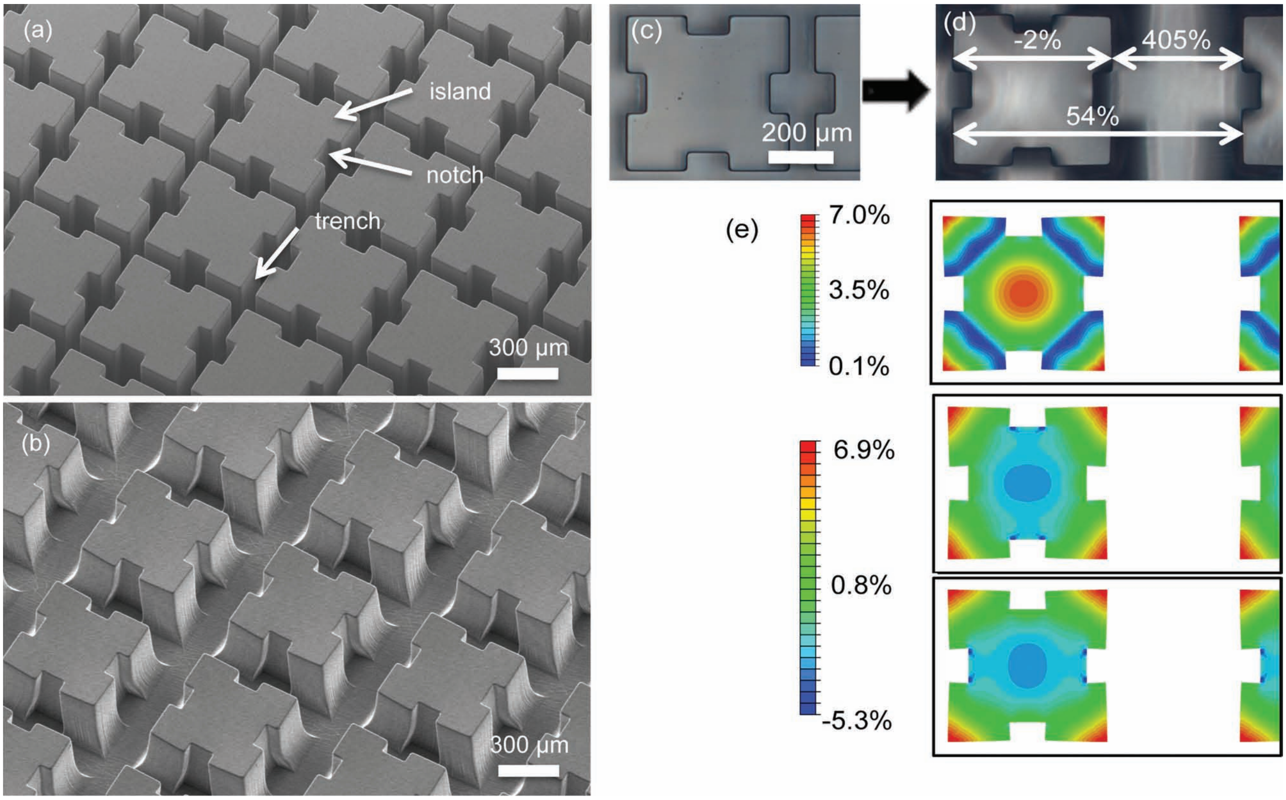

Figure 1. Scanning electron microscopy (SEM) images, optical microscopy images, and finite element modeling (FEM) of a slab of poly(dimethylsiloxane) (PDMS) with surface relief in the geometry of an array of notched islands. This structure serves as a platform for stretchable inorganic photovoltaic modules, in which microscale solar cells (microcells) mount on top of the islands, with ribbon-shaped interconnects that span the trenches at the locations of the notches. The design enables high levels of stretchability and areal coverage, in formats that provide both strain-isolation and strain-limiting behavior. a) SEM image of a PDMS substrate with an array of notched islands (each ~500 μm × 500 μm), separated by recessed trenches (widths ~76 μm, depths ~350 μm). The notches (~120 μm × 60 μm) accommodate the interconnects, in a way that maximizes their lengths (for large stretchability) while sacrificing minimal areal coverage and retaining space between islands, even at extreme levels of deformation. b) SEM image of this substrate in a biaxially stretched state. The relatively thin base layers in the regions of the trenches, compared to those in the islands regions, localize strain to the trenches. Furthermore, the strain in the islands decreases from bottom to top. These two effects result in minimal strains on the top surfaces of the islands, where the microcells are mounted. c,d) Optical microscopy images of the substrate in relaxed (c) and stretched (d) states. The latter image shows that stretching (in this case, overall applied strain of 54%) induces dimensional changes at the top surfaces of the islands (approximately −2%) that are much smaller than those at the trenches (~405%). e) FEM results of the distribution of maximum principal strain and the two components of the strain tensor at the top surfaces of adjacent islands. The computed elongations are −1.7% and 416% at the top surfaces and the trenches, respectively, for an overall applied strain of 54%. These results match well with the experiments.

both strain isolation and strain-limiting behavior. Figure 1a presents a representative case of a poly(dimethylsiloxane) (PDMS) substrate formed by soft lithographic molding against a corresponding master defined by photolithography. For this example, the lateral dimensions of the islands are ~500 μm × 500 μm, separated by trenches with widths of ~76 μm. The notches on the islands have widths of ~120 μm and depths of ~60 μm. The height of the islands and the thickness of the underlying base layer are 350 and 160 μm, respectively. The areal coverage of the islands, each of which supports an individual microcell, corresponds to 67% of the overall area. (i.e., $\sim(500-4\times120\times60)^2/(500+76)^2$). The total, edge-to-edge distance between the inner parts of the notches on adjacent islands is 196 μm (i.e., ~60 + 76 + 60 μm). This feature is important because it increases the lengths of interconnect structures that span the trenches to bridge adjacent microcells, compared to the analogous case of square islands without notches as described previously.[29] This increase in length translates directly to a corresponding reduction in the strains experienced by the interconnects upon deformation. Figure 1b shows an angled view of a substrate stretched biaxially to an overall strain of 37%. The small substrate thickness at the trenches reduces the cross sectional area, thereby leading to localization of strains to these regions when stretching/deforming the overall system. Furthermore, the strain at the islands monotonically decreases from their base areas to their top surfaces, resulting in minimal strain at the locations that support the microcells. This design, which includes notches and large relief, represents an advanced embodiment of a design strategy reported recently,[29] for improved areal coverage at a given range of stretchability. In particular, for the example described here, the structured substrate improves the overall stretchability by nearly three times compared to previous results, at similar levels of areal coverages of island regions. As shown in Figure 1c and d, such a substrate subjected to an overall tensile strain of ~54% undergoes elongations (~405%) in the trenches that are much higher (>200 times) than those at the islands (approximately –2%). The corresponding elongations obtained by the finite element method (FEM) are 416% and –1.7%, which compare well with the experimental results. We expect that the small negative strain could be reduced to zero through appropriate selection of the heights of islands.[29]

The notches offer another, and qualitatively distinct, advantage: they provide space for the interconnects even when the substrate is deformed to an extent that brings the top surface edges of adjacent islands into physical contact. This type of strain-limiting behavior avoids damage that would occur to the interconnects in otherwise similar designs that do not include the notches. **Figure 2**a shows, for example, bending of a structured substrate by wrapping on a cylinder with radius of 3.6 mm. The image clearly illustrates that the outer edges of the islands in this case touch each other but the edges of notches do not, thus securing spaces for interconnects. The FEM results in Figure 2b indicate that the top surfaces of the islands are relatively flat and experience low strain (approximately –0.5%). The other frames of Figure 2 show SEM images and FEM results for various other states of deformation. A substrate under uniaxial strain of 18% appears in Figure 2c. The trenches elongate by 139% along the direction of stretching, then they contract by 71% in the orthogonal direction due to the Poisson effect. As with the case of Figure 2a, even though the width of the trenches reduces to very small dimensions (~22 µm), the lateral space for interconnects is still relatively large (~142 µm) due to the presence of the notches, thereby preventing breakage from excessive strain. The FEM results as shown in Figure 2d for this case indicate strains of 154% and –64% in the trenches along and perpendicular to the stretching direction. Figure 2e and f show an SEM image and FEM results for outward bending by wrapping on a cylinder with a radius of 1.5 mm. The base of the substrate and region near the bottom of the islands absorb the bending strains, while keeping the top surface of islands flat with minimal strain. Here, the strain computed by FEM is -1.7% at the top surface of the islands, which is much smaller than that at the trenches (214%). The image in Figure 2g shows a substrate twisted by 60° over a length of 3.46 mm. The corresponding FEM (Figure 2h) indicates minimal strain (approximately –0.8%) on the top surfaces of the islands.

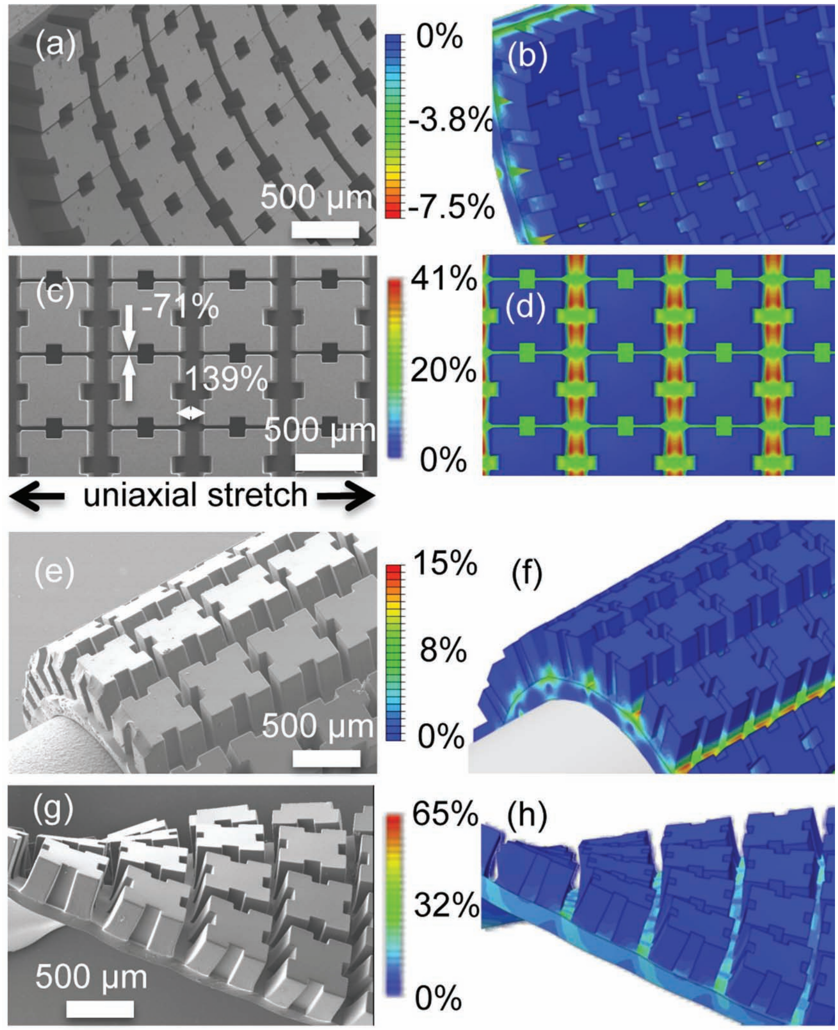

Figure 2. SEM images and FEM results for PDMS substrates with surface relief in the form of notched islands, in several deformed configurations. a) SEM image and b) FEM results for a substrate bent inward by wrapping on a cylinder with radius of 3.6 mm. Here, the top edges of adjacent islands come into physical contact, but the notches maintain some space for the interconnect structures. c) Uniaxial stretching (18%) results in narrowing of the widths of the trenches (~71%) in the direction perpendicular to the stretching, due to the Poisson effect. The image shows that the notches maintain space between the islands to accommodate the interconnects, even in the case of extreme narrowing. d) FEM results of the distribution of strain at the top surface of the PDMS, for uniaxial stretching. These computations show 154% elongation and 64% narrowing in the trenches along and perpendicular to the direction of applied strain of 18%, respectively. e) SEM image and f) FEM results for a substrate bent outward by wrapping onto a cylinder with a radius of 1.5 mm. The strain at the top surface of the island (–1.7%) is much smaller than that (~214%) at the trenches. g) SEM image and h) FEM results for a substrate twisted by 60° over a length of 3.46 mm. The effects of strain isolation are apparent.

As a module demonstration, we exploited these optimized substrates as supports for interconnected arrays of dual-junction GaInP/GaAs microcells (total thickness ~6.14 µm). The fabrication begins with defining lateral dimensions of notched microcells (size: ~460 µm × 460 µm, notch: ~160 µm × 60 µm) from epitaxially layers grown on GaAs wafers, and

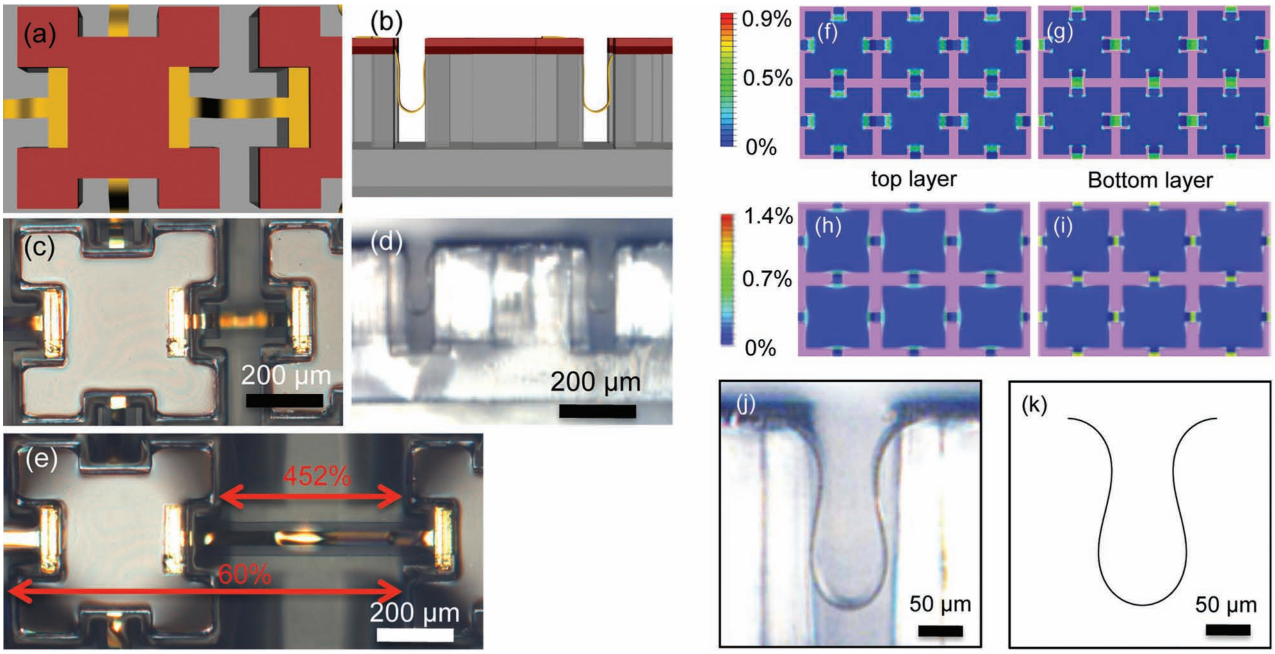

Figure 3. Schematic illustrations of stretchable GaInP/GaAs photovoltaic modules, optical microscopy images, and FEM results. a) Top and b) side view of each unit cell, showing a notched dual-junction GaInP/GaAs microcell (size: ~460 µm × 460 µm, notch: ~160 µm × 60 µm, thickness: ~6.14 µm) aligned and mounted on a PDMS island, configured with top (n) and bottom (p) contacts that connect to thin electrical interconnect ribbons which buckle down into the recessed trenches upon relaxation of the pre-strain applied to the PDMS during the fabrication. c,d) Optical microscopy image of a corresponding region of a module viewed from top (c) and side (d) in the as-fabricated state. The areal coverage of the microcells is 67%. e) Similar region of the same device, in a state of 60% overall biaxial strain. The interconnects move to accommodate fractional increases in the widths of the trenches by ~452%. f,g) FEM results of the top (f) and bottom (g) surfaces of the layers of Au in the interconnects, for a module in its relaxed state. These maximum principal strains are 0.32% and 0.36% at the top and bottom surfaces, corresponding to values more than 100 times smaller than the applied strain (60%). h,i) With square islands, in otherwise similar layouts and areal coverages, the maximum principal strains are 0.40% and 0.47% at the top and bottom surfaces, respectively. The neutral mechanical plane configuration of the interconnects helps to ensure that these strains are low, in both cases. j,k) The profiles of buckled interconnect in experiments and analytical model, which agree very well.

then etching them to expose n and p contacts. Releasing the cells by eliminating an underlying sacrificial layer in the epitaxial stack, and then transfer-printing arrays of the microcells onto a plastic substrate prepares them for electrical and mechanical interconnection into open mesh geometries. (See details in the Experimental Section) Aligned transfer printing delivers the resulting open mesh structure onto a prestrained structured PDMS and relaxing the prestrain completes the process. **Figure 3**a and b present top and side views of each unit cell, showing a notched dual-junction GaInP/GaAs microcell mounted on a PDMS island. The areal coverage of the devices is 67% in the relaxed state. Figure 3c and d show optical microscopy images of the completed module from top and side views, respectively. The module is stretchable up to 60% biaxially as shown in Figure 3e. The arc-shaped interconnects, which buckle down into the trenches between the notches, straighten to accommodate strains of up to 452% between trenches. The strain in the interconnects is given analytically in terms of the overall strain, ε (see the Supporting Information (SI)).

$$\varepsilon_{\text{interconnect}} = \frac{8y \sin\frac{\alpha}{2} K\left(\sin\frac{\alpha}{2}\right)}{\varepsilon w_{\text{island}} + (1+\varepsilon)\, w_{\text{trench}} + 2w_{\text{notch}}} \tag{1}$$

where y is the distance to the neutral mechanical plane of interconnect, w_{notch}, w_{trench}, and w_{island} are the widths of notch, trench, and island, respectively, and $K(k) = \int_0^{\pi/2} \frac{d\phi}{\sqrt{1-k^2\sin^2\phi}}$ is the complete elliptic integral of the first kind, where α is the maximum rotation angle of interconnect determined by

$$2\frac{E\left(\sin\frac{\alpha}{2}\right)}{K\left(\sin\frac{\alpha}{2}\right)} = 1 + \frac{w_{\text{trench}} + 2w_{\text{notch}}}{\varepsilon w_{\text{island}} + (1+\varepsilon)\, w_{\text{trench}} + 2w_{\text{notch}}} \tag{2}$$

and $E(k) = \int_0^{\pi/2} \sqrt{1-k^2\sin^2\phi}\, d\phi$ is the complete elliptic integral of the second kind. For w_{notch} = 60 µm, w_{trench} = 76 µm, w_{island} = 500 µm, and ε = 60%, the maximum strain in the Au layer of interconnect is 0.36%. For the corresponding case of square islands without notches, at the same areal coverage and level of stretchability, w_{trench} = 111 µm, w_{island} = 500 µm, and ε = 60%, the maximum strain in the Au layer of interconnect is 0.46%. These results are consistent with corresponding outcomes from FEM in Figure 3f–i (i.e., 0.36% and 0.47% for notched and square island designs, respectively).

A notable feature of the mechanics is that, unlike classical Euler-type buckling, the interconnect takes on a non-sinusoidal shape due to extremely large levels of compression. The modified buckling profile can be obtained analytically, according to the parametric equation

$$x = \bar{x}(\varphi), \quad y = \bar{y}(\varphi), \tag{3}$$

where (x,y) are the Cartesian coordinates, the parameter φ ranges from 0 to $\pi/2$, and the functions $\bar{x}$ and $\bar{y}$ are given in the SI. Figure 3j shows that the experimental profile of a buckled interconnect for w_{notch} = 60 µm, w_{trench} = 76 µm, w_{island} = 500 µm, and ε = 60%, agrees well with the analytical result in Figure 3k.

The properties of the solar cells (without antireflection coatings) were determined using an automated spectroradiometric measurement system (OL 750 Optronic Laboratories) and a solar simulator (Oriel, 91192). **Figure 4**a shows external quantum efficiency (EQE), internal quantum efficiency (IQE), and reflectance results. The EQE is ~68% and the reflectance is ~28%, for both GaInP and GaAs layers. The IQE is ~95%, also for both layers. Figure 4b shows current–voltage (I–V) characteristics of a completed dual-junction GaInP/GaAs microcells in a notched geometry. The short-circuit current density (J_{sc}) and open-circuit voltage (V_{oc}) are 9.8 mA/cm^2 and 2.28 V, respectively. The energy conversion efficiency (η) and fill factor (FF) are 19% and 0.85, respectively. Since the reflectance is ~28% of the incident light, we expect that the efficiency can be improved to ~25% with an optimized ARC. The notched island design implemented with 2 J solar microcells offers considerably higher conversion efficiency, in addition to improved degrees of stretchability, compared to single-junction microcell systems reported previously.[29,30] The concepts reported here have the potential to be useful for a range of other applications, due to their applicability to many classes of semiconductor devices, from light emitting diode displays/lighting systems to digital imagers, integrated circuits and others.

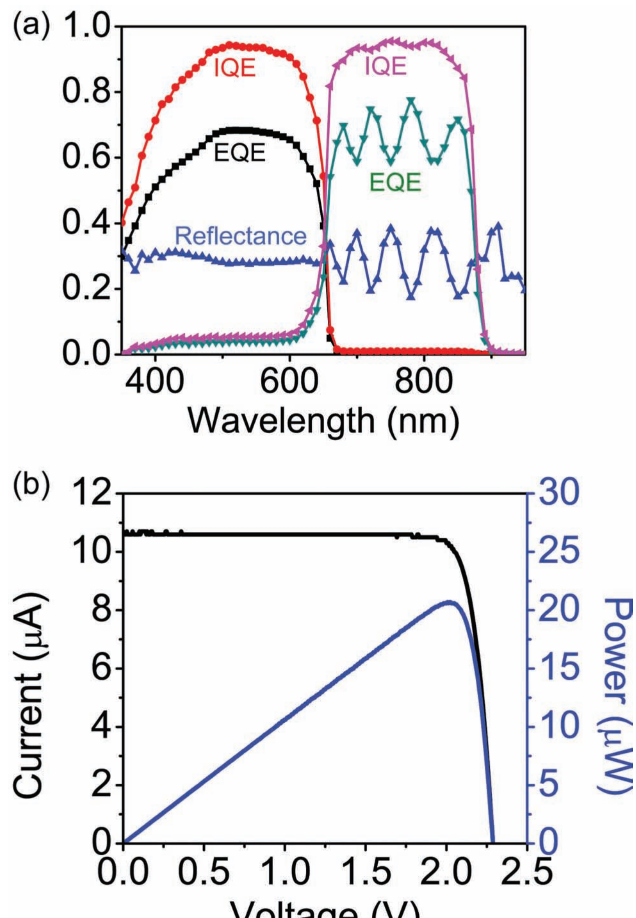

Figure 4. Electrical characteristics of a stretchable photovoltaic module consisting of notched GaInP/GaAs dual-junction microcells on a PDMS substrate with similarly notched relief designs. a) Internal quantum efficiency (IQE), external quantum efficiency (EQE), and reflectance of a representative cell, without anti-reflection coating (ARC). The EQE and reflectance are ~68% and ~28%, respectively. The IQE is ~95%, for both top (GaInP) and bottom (GaAs) junctions, indicating that the structure makes efficient use of absorbed light. b) Current–voltage characteristics. The short circuit current density (J_{sc}), open circuit voltage (V_{oc}), fill factor (FF), and conversion efficiency (η) are 9.8 mA/cm^2, 2.28 V, 0.85, and 19%, respectively. Improvements the short-circuit current and conversion efficiency are possible with the addition of an ARC up to estimated values of ~12 mA/cm^2 and ~25%, respectively.

Experimental Section

Structured PDMS: The structured PDMS substrates were formed by casting and curing prepolymer to a silicone elastomer (10:1 mixture of base and curing agent, Sylgard 184, Dow Corning) against a photolithographically defined pattern of SU8 (~350 µm) on a silicon wafer.[31] Release of the cured PDMS yielded structured substrates with rectangle notches (each ~120 µm × 60 µm) on each sidewall. The notched islands have dimensions of ~500 µm × 500 µm, separated by recessed trenches with widths ~76 µm and depths ~350 µm. The thickness of the underlying base is ~160 µm, defined by weighing the amount of prepolymer applied to the patterned SU8.

Fabricating Solar Microcells: Fabrication of dual-junction, GaInP/GaAs solar microcells began with sequential chemical wet etching of the GaInP and GaAs layers of a specialized epitaxial stack on a GaAs wafer with hydrochloric acid (HCl, 37%, Fisher Scientific) and phosphoric acid (H_3PO_4, 85%, Fisher Scientific), respectively. Details of the epitaxial stack layout appear in the SI. Sequential electron beam deposition of Ti (20 nm) and Au (60 nm) on the n and p regions of the microcells formed Ohmic contacts. Spin-cast positive photoresist encapsulated the defined microcells completely. Photolithography defined holes around the periphery of the microcells to expose the underlying sacrificial layer. Chemical etching removed the sacrificial layer; the photoresist protected the microcells from unwanted etching during this process.

Transfer Printing and Interconnection: Transfer printing with a PDMS stamp (Sylgard 184, Dow Corning) delivered the microcells onto a layer of epoxy (0.5 µm, SU8, Microchem) spin cast on a film of poly(methylmethacrylate) (1 µm, PMMA) on a carrier wafer. A bilayer of Ti (20 nm) and Au (300 nm) patterned on a film of SU8 (0.5 µm) with openings in the n- and p-contact regions provided series interconnects between the microcells. Spin casting another layer of SU8 (1 µm) on top as an encapsulant located the Ti/Au near the neutral mechanical plane. See the SI for more detailed discussion of the configurations of the interconnects. Reactive ion etching (CS-1701, March, 150 mTorr, 150 W, O_2 ~20 sccm, 50 min) of the SU8 layer through a patterned etch mask of SiO_2 formed an open mesh structure of islands and bridges on the carrier wafer. Another transfer printing step lifted the interconnected mesh of GaInP/GaAs solar microcells after dissolving the underlying layer of

PMMA in acetone. Depositing layers of Ti (5 nm) and SiO_2 (30 nm) on the back surface of the mesh prepared the system for bonding onto a prestrained, structured substrate of PDMS, treated with UV ozone to create –OH groups for the required surface chemistry. An assembly of translation and rotation stages, and an optical microscope enabled accurate alignment.

Electrical Characteristics: The EQE and IQE were measured with an automated spectroradiometric measurement system (OL 750 Optronic Laboratories) by exposing a solar cell (~2 mm × 2 mm) to monochromatic light. The *I–V* data from the solar microcells were evaluated under a 1000 W full spectrum solar simulator (Oriel, 91192) using a DC sourcemeter (model 2400, Keithley).

Supporting Information

Supporting Information is available from the Wiley Online Library or from the author.

Acknowledgements

We thank R. H. Kim and I. Jung for invaluable discussions. We also thank J. Soares for help with the measurements of quantum efficiency. This material is based upon work supported by the Office of Naval Research. J. Lee acknowledges support from the "Basic Research Projects in High-tech Industrial Technology" Project through a grant provided by GIST in 2012.

[1] D. S. Gray, J. Tien, C. S. Chen, *Adv. Mater.* **2004**, *16*, 393.
[2] S. P. Lacour, J. Jones, S. Wagner, T. Li, Z. G. Suo, *Proc. IEEE* **2005**, *93*, 1459.
[3] D. Brosteaux, F. Axisa, M. Gonzalez, J. Vanfleteren, *IEEE Electron Device Lett.* **2007**, *28*, 552.
[4] M. Gonzalez, F. Axisa, M. V. BuIcke, D. Brosteaux, B. Vandevelde, J. Vanfleteren, *Microelectron. Reliability* **2008**, *48*, 825.
[5] D. H. Kim, J. Z. Song, W. M. Choi, H. S. Kim, R. H. Kim, Z. J. Liu, Y. Y. Huang, K. C. Hwang, Y. W. Zhang, J. A. Rogers, *Proc. Nat. Acad. Sci. USA* **2008**, *105*, 18675.
[6] D. H. Kim, Z. J. Liu, Y. S. Kim, J. Wu, J. Z. Song, H. S. Kim, Y. G. Huang, K. C. Hwang, Y. W. Zhang, J. A. Rogers, *Small* **2009**, *5*, 2841.
[7] J. A. Rogers, T. Someya, Y. Huang, *Science* **2010**, *326*, 1603.
[8] D. Y. Khang, H. Jiang, Y. Huang, J.A. Rogers, *Science* **2006**, *311*, 208.
[9] D.-H. Kim, J.-H. Ahn, W.-M. Choi, H.-S. Kim, T.-H. Kim, J. Song, Y. Y. Huang, L. Zhuangjian, L. Chun, J. A. Rogers, *Science* **2008**, *320*, 507.
[10] T. Sekitani, Y. Noguchi, K. Hata, T. Fukushima, T. Aida, T. Someya, *Science* **2008**, *321*, 1468.
[11] T. Sekitani, H. Nakajima, H. Maeda, T. Fukushima, T. Aida, K. Hata, T. Someya, *Nat. Mater.* **2009**, *8*, 494.
[12] L. Hu, M. Pasta, F. L. Mantia, L. Cui, S. Jeong, H. D. Deshazer, J. W. Choi, S. M. Han, Y. Cui, *Nano Lett.* **2010**, *10*, 708.
[13] T. Takahashi, K Takei, A. G. Andrew, F. S. Fearing, A. Javey, *Nano Lett.* **2011**, *11*, 5408.
[14] X. Wang, H. Hu, Y. Shen, X. Zhou, Z. Zheng, *Adv. Mater.* **2011**, *23*, 3090.
[15] Z. Yu, X. Niu, Z. Liu, Q. Pei, *Adv. Mater.* **2011**, *23*, 3989.
[16] D. J. Lipomi, B. C.-K. Tee, M. Vosgueritchian, Z. Bao, *Adv. Mater.* **2011**, *23*, 1771.
[17] P. Görrn, W. Cao, S. Wagner, *Soft Matter* **2011**, *7*, 7177.
[18] J. A. Rogers, M. G. Lagally, R. G. Nuzzo, *Nature* **2011**, *477*, 45.
[19] S.-I. Park, Y. Xiong, R.-H. Kim, P. Elvikis, M. Meitl, D.-H. Kim, J. Wu, J. Yoon, C.-J. Yu, Z. Liu, Y. Huang, K.-C. Hwang, P. Ferreira, X. Li, K. Choquette, J. A. Rogers, *Science* **2009**, *325*, 977.
[20] R.-H. Kim, D.-H. Kim, J. Xiao, B. H. Kim, S.-I. Park, B. Panilaitis, R. Ghaffari, J. Yao, M. Li, Z. Liu, V. Malyarchuk, D. G. Kim, A.-P. Le, R. G. Nuzzo, D. L. Kaplan, F. G. Omenetto, Y. Huang, Z. Kang, J. A. Rogers, *Nat. Mater.* **2010**, *9*, 929.
[21] H. Kim, E. Brueckner, J. Song, Y. Li, S. Kim, C. Lu, J. Sulking, K. Choquette, Y. Huang, R. G. Nuzzo, J. A. Rogers, *Proc. Nat. Acad. Sci. USA* **2011**, *108*, 10072.
[22] H. C. Ko, M. P. Stoykovich, J. Song, V. Malyarchuk, W. M. Choi, C.-J. Yu, J. B. Geddes, J. Xiao, S. Wang, Y. Huang, J. A. Rogers, *Nature* **2008**, *454*, 748.
[23] G. Shin, I. Jung, V. Malyarchuk, J. Song, S. Wang, H. C. Ko, Y. Huang, J. S. Ha, J. A. Rogers, *Small* **2010**, *6*, 851.
[24] H. C. Ko, G. Shin, S. Wang, M. P. Stoykovich, J. W. Lee, D.-H. Kim, J. S. Ha, Y. Huang, K.-C. Hwang, J. A. Rogers, *Small* **2009**, *5*, 2703.
[25] B. P. Timko, T. Cohen-Karni, G. H. Yu, Q. Qing, B. Z. Tian, C. M. Lieber, *Nano Lett.* **2009**, *9*, 914.
[26] J. Viventi, D. H. Kim, J. D. Moss, Y. S. Kim, J. A. Blanco, N. Annetta, A. Hicks, J. L. Xiao, Y. G. Huang, D. J. Callans, J. A. Rogers, B. Litt, *Sci. Transl. Med.* **2010**, *2*, 24ra22.
[27] D.-H. Kim, N. Lu, R. Ma, Y.-S. Kim, R.-H. Kim, S. Wang, J. Wu, S. M. Won, H. Tao, A. Islam, K. J. Yu, T.-I. Kim, R. Chowdhury, M. Ying, L. Xu, M. Li, H.-J. Chung, H. Keum, M. McCormick, P. Liu, Y.-W. Zhang, F. G. Omenetto, Y. Huang, T. Coleman, J. A. Rogers, *Science* **2011**, *333*, 838.
[28] D.-H. Kim, J. Xiao, J. Song, Y. Huang, J. A. Rogers, *Adv. Mater.* **2010**, *22*, 2108.
[29] J. Lee, J. Wu, M. Shi, J. Yoon, S.-I. Park, M. Li, Z. Liu, Y. Huang, J. A. Rogers, *Adv. Mater.* **2011**, *23*, 986.
[30] J. Yoon, S. Jo, I. S. Chun, I. Jung, H.-S. Kim, M. Meitl, E. Menard, X. Li, J. J. Coleman, U. Paik, J. A. Rogers, *Nature* **2010**, *465*, 329.
[31] Y. N. Xia, G. M. Whitesides, *Ann. Rev. Mater. Sci.* **1998**, *28*, 153.

Received: November 21, 2011
Revised: January 13, 2012
Published online: March 29, 2012